In Vitro Cell.Dev.Biol.—Animal (2014) 50:56–65
DOI 10.1007/s11626-013-9678-1

Establishment and characterization of a primary and a metastatic melanoma cell line from Grey horses

Monika H. Seltenhammer · Elisabeth Sundström · Claudia Meisslitzer-Ruppitsch · Petra Cejka · Jedrzej Kosiuk · Josef Neumüller · Marlene Almeder · Otto Majdic · Peter Steinberger · Udo M. Losert · Johannes Stöckl · Leif Andersson · Johann Sölkner · Monika Vetterlein · Anna Golovko

Received: 23 January 2013 / Accepted: 30 July 2013 / Published online: 28 August 2013 / Editor: T. Okamoto

Abstract The Grey horse phenotype, caused by a 4.6 kb duplication in *Syntaxin 17*, is strongly associated with high incidence of melanoma. In contrast to most human melanomas with an early onset of metastasis, the Grey horse melanomas have an extended period of benign growth, after which 50% or more eventually undergo progression and may metastasize. In efforts to define changes occurring during Grey horse melanoma progression, we established an in vitro model comprised of two cell lines, HoMel-L1 and HoMel-A1, representing a primary and a metastatic stage of the melanoma, respectively. The cell lines were examined for their growth and morphological characteristics, in vitro and in vivo oncogenic potential, chromosome numbers, and expression of melanocytic antigens and tumor suppressors. Both cell lines exhibited malignant characteristics; however, the metastatic HoMel-A1 showed a more aggressive phenotype characterized by higher proliferation rates, invasiveness, and a stronger tumorigenic potential both in vitro and in vivo. HoMel-A1 displayed a near-haploid karyotype, whereas HoMel-L1 was near-diploid. The cell lines expressed melanocytic lineage markers such as TYR, TRP1, MITF, PMEL, ASIP, MC1R, POMC, and KIT. The tumor suppressor p53 was strongly expressed in both cell lines, while the tumor suppressors p16 and PTEN were absent in HoMel-A1, potentially implicating significance of these pathways in the melanoma progression. This in vitro model system will not only aid in understanding of the Grey horse melanoma pathogenesis, but also in unraveling the steps during melanoma progression in general as well as being an invaluable tool for development of new therapeutic strategies.

M. H. Seltenhammer
Department of Forensic Sciences, Schwarzspanierstrasse 17, 1090 Vienna, Austria

M. H. Seltenhammer
Center of Physiology and Pharmacology, Vasco-Bio-Laboratory, Medical University of Vienna, Lazarettgasse 19, 1090 Vienna, Austria

M. H. Seltenhammer
Department of Pharmacology and Toxicology, University of Vienna, Althanstrasse 14, 1090 Vienna, Austria

E. Sundström · L. Andersson · A. Golovko (✉)
Science for Life Laboratory Uppsala, Department of Medical Biochemistry and Microbiology, Uppsala University, Box 582, 751 23 Uppsala, Sweden
e-mail: anna.golovko@imbim.uu.se

C. Meisslitzer-Ruppitsch · J. Kosiuk · J. Neumüller · M. Almeder · M. Vetterlein
Department of Cell Biology and Ultrastructure Research, Center for Anatomy and Cell Biology, Medical University of Vienna, Schwarzspanierstrasse 17, 1090 Vienna, Austria

P. Cejka · O. Majdic · P. Steinberger · J. Stöckl
Institute of Immunology, Medical University of Vienna, Schwarzspanierstrasse 17, 1090 Vienna, Austria

U. M. Losert
Core Unit for Biomedical Research, Medical University of Vienna, Schwarzspanierstrasse 17, 1090 Vienna, Austria

L. Andersson
Department of Animal Breeding and Genetics, Swedish University of Agricultural Sciences, Box 597, 751 24 Uppsala, Sweden

J. Sölkner
Department of Sustainable Agricultural Systems, University of Natural Resources and Applied Life Sciences, 1180 Vienna, Austria

Keywords Grey horse · Primary and metastatic melanoma · Cell lines · In vitro model · Tumor suppressor

Introduction

The Grey horse phenotype is strongly associated with a high incidence of melanoma. It has been estimated that almost 80% of Grey horses older than 15 yr develop melanomas (Sutton and Coleman 1997), which occur as jet-black, firm, well-circumscribed nodules primarily in the dermis of glabrous skin of the ventral site of the tail and in the anal, perianal and genital regions, perineum, lips, and eyelids, but can also occur internally (Valentine 1995; Fleury et al. 2000; Seltenhammer et al. 2004). At the onset, the primary multiple melanomas show benign behavior; however, about 66% of the tumors may eventually undergo progression and metastasize into the surrounding tissue (e.g., occur at atypical sites), lymph nodes, and internal organs (Gorham and Robl 1986; MacGillivray et al. 2002). As histopathology is not sufficient to predict the metastatic potential of the tumors (Valentine 1995; Fleury et al. 2000; Seltenhammer et al. 2004), a reliable marker system needs to be established.

We have previously identified a 4.6 kb intronic duplication in the *Syntaxin 17* (*STX17*) gene as the causative mutation for the Grey horse phenotypes including melanoma development (Rosengren Pielberg et al. 2008). Further functional studies revealed that the duplicated sequence contains an enhancer element, and that the duplication transforms this element from a weak to a strong melanocyte-specific element that upregulates the expression of both *STX17* and the neighboring *NR4A3* gene (Sundström et al. 2011). Interestingly, we observed a copy number expansion of the *STX17* duplication in more aggressive tumors, suggesting that the duplication is a melanoma-driving element (Sundström et al. 2012). To comprehensively study the mechanistic link between the *STX17* duplication and the Grey horse melanoma (GHM) development, a convenient model system is essential.

In vitro cell culture lines representative of different stages of GHM would provide such a system in which to study the molecular mechanisms of the disease, find new markers of the melanoma progression, and test new therapeutical strategies. To date, a few long-term growing cell lines from primary GHM tumors have been established (Chapman et al. 2009), whereas culturing of cells from metastatic tumors has not been yet described. Here, we report the establishment and characterization of two permanently growing cell lines representing a primary and a metastatic stage of Grey horse melanoma.

Material and Methods

Establishment of cell lines. Excision of the melanoma tumors was performed according to standard surgical methods. A deeply pigmented, firm, well-circumscribed homogenous primary dermal melanoma tumor with a size of 15×15×12 cm was excised from the ventral side of the tail of a 25-yr-old Lipizzaner stallion (HoMel-L1). A relapsing, proximal to the primary site, nonhomogeneous, partly unpigmented, ulcerating, and fast growing dermal–epidermal skin metastasis with a size of 14×10×10 cm was excised from the dorsal side of the tail of an 18-yr-old Shagya-Arabian mare (HoMel-A1). The tumors were minced mechanically in phosphate-buffered saline (PBS; Invitrogen, Lofer, Austria). Each resulting suspension, containing only few single cells and small tissue fragments, was extensively washed in PBS for several times in order to remove melanin. After the last centrifugation, the pellets were resuspended in RPMI-1640 medium (Invitrogen) containing 10% fetal bovine serum (Invitrogen) and antibiotics (GIBCO^{TM} antibiotic–antimycotic 100X liquid; Invitrogen). The suspensions were seeded in tissue culture flasks and incubated at 37°C in a humid atmosphere of 5% CO_2 in air. The cultures were left for up to 2 wk almost undisturbed to facilitate the adaptation of cultures to in vitro conditions, as well as the attachment of cells and tissue fragments. Thereafter, medium was changed once a wk. Routine assays for *Mycoplasma* using a MycoAlert™ *Mycoplasma* detection kit (Lonza Bioscience, Stockholm, Göteborg) were negative.

In vitro proliferation. Growth characteristics in monolayer cultures were determined after at least ten culture passages using a commercially available proliferation assay (Quick Cell Proliferation assay kit II; BioVision, Milpitas, CA) according to the manufacturer's instructions.

Light and transmission electron microscopy. For light microscopy, cells were examined as 80% confluent cultures in bright field and phase contrast to investigate cytoplasmatic and membrane morphology, respectively (NIKON Eclipse TE 300, Vienna, Austria).

For transmission electron microscopy of cells, cultures were prepared as described (Cengelli et al. 2009). Subsequently, cells were fixed in 0.25% buffered glutaraldehyde (Sigma-Aldrich, Vienna, Austria), incubated in osmium tetroxide, rinsed in increasing concentrations of hexylene glycol (30, 50, 70, 90, and 100%) and embedded into epoxy cast (JEOL TEM Transmission electron microscope, Vienna, Austria).

Giemsa–Wright staining. The cells grown on cover slips were fixed in methanol for 10 min and stained with Giemsa–Wright stain (Sigma-Aldrich) for 2 min and then with five times diluted Giemsa–Wright stain for additional 2 min,

washed with dH_2O, and observed for nuclear and cytoplasmic morphology (NIKON Eclipse TE 300).

Determination of chromosome numbers. Chromosome numbers of each cell line were determined according to standard procedure. Briefly, to the cells of each line in log growth phase, 60–80% confluent, Colcemid (Boehringer Mannheim; 10 μg/ml, Vienna, Austria) was added to a final concentration of 0.1 μg/ml and incubated at 37°C, 5%CO_2 for 45 min. Subsequently, the cells were detached by trypsin/EDTA, centrifuged, and treated with hypotonic solution (0.075 M potassium chloride). After incubation for 15 min in 37°C water bath, reaction was stopped by adding fixative solution (3:1—methanol/acetic acid). After another centrifugation step, cells were incubated in fixative solution and centrifuged. Chromosomes were prepared on slides and stained with either DAPI or Quinacrine-HCl (Sigma-Aldrich) according to manufacturer's guidelines. Documentation was carried out with fluorescence microscopy (NIKON Eclipse TE 300).

Colony forming assay. To investigate the colony forming capability of HoMel-L1 and HoMel-A1 cultures, 150–200 single cell suspensions of each cell line in 0.8 ml growth media containing 0.3% low-melting agarose (Sigma-Aldrich) were plated in triplicates in 24-well plates over a base layer of 0.8 ml growth media containing 0.6% low-melting agarose. The plates were incubated for 15–17 d or until colonies were formed. Colony diameters larger than 70 μm or colonies containing more than 45 cells were then counted as 1 positive colony using light microscopy (NIKON Eclipse TE 300).

Matrigel invasion assay. The Matrigel invasion chambers (Becton Dickinson, Franklin Lakes, NJ) were used to assess the invasive potential of HoMel-L1 and HoMel-A1 cultures essentially according to the manufacturer's instructions. Briefly, the control and test inserts were rehydrated for 2 h in the cell culture incubator in 24-well plates with 500 μl serum-free DMEM in the well and 500 μl in the insert. After rehydration, about 3×10^4 cells of each line in 500 μl of complete DMEM were seeded in each of the control and test inserts. Seven hundred fifty microliter of DMEM with 10% FCS was served as chemoattractant in the bottom of each well. The plates were incubated for 24 h in the cell culture incubator. The cells on the inserts were fixed in 4% PBS-buffered paraformaldehyde, washed in PBS, stained with Giemsa–Wright stain (Sigma-Aldrich, St Louis, MO) for 30 min, and washed in dH_2O. The cells on the top of insert's membranes were removed with several Q-tips. Invading cells were counted in three microscopic fields using a ten × objective.

The percentage of invasion was determined as the mean number of invading cells in the test membrane/number of the cells migrating through the control membrane × 100. The assay was performed in sextuplicates and repeated twice.

In vivo tumor growth in SCID mice. Six-week-old female severe combined immunodeficient (SCID) mice were xenografted by injecting 1.5×10^6 cells in 200 μl PBS of each cell line subcutaneously into the interscapular region. Non-tumorigenic equine fibroblast served as negative control. Five animals of each group were injected and observed over a period of 16 weeks. SCID mice were obtained from The Jackson Laboratory and bred and housed according to the guidelines of the Medical University of Vienna, Division of Comparative Medicine. The animal ethics committee approved all the experiments. For each group of mice, the data were described using the mean value of each group and its associated standard deviation. The tumor volumes were calculated as tumor size**3*pi/6 (SAS 2011). The statistical comparisons were performed using the Student's t test for the difference between group experiment and group control. Value of $P<0.05$ was considered statistically significant.

Immunofluorescence. The cells were grown on glass coverslips for 1–3 d, fixed in 2.4% PBS-buffered paraformaldehyde, and permeabilized in 0.2% Triton X-100. Subsequently, the cells were incubated with the following primary antibodies: anti-TRP1, anti-TYR, and anti-TRP2–rabbit polyclonal (Santa Cruz Biotechnology, Inc., Heidelberg, Germany), anti-AP-2α, anti-MITF–mouse monoclonal (Santa Cruz Biotechnology, Inc.), and anti-PMEL–rabbit affinity-purified polyclonal (Raposo et al. 2001). Respective fluorescent Alexa Fluor 488 and Texas Red-X secondary antibodies were used for visualization of the signals (Molecular Probes, Invitrogen, Life Tech Austria, Vienna, Austria). Antigen expression was analyzed by fluorescence microscopy (NIKON Eclipse TE 300).

Western blot analysis. Cells were lysed in a buffer containing 50 mM Tris (pH 7.5), 100 mM NaCl, 1 mM EDTA, 10% glycerol, 20 mM sodium fluoride, 2.5 mM sodium pyrophosphate, 1 mM sodium orthovanadate, and 0.5% Triton X-100 with a protease- and phosphatase-inhibitor cocktails (Roche Diagnostics, Mannheim, Germany). Immunoblotting was performed with antibodies against mouse monoclonal anti-p16 (clone G175-405, BD Pharmingen), mouse monoclonal anti-p53 (clone Pab240, Calbiochem, Darmstadt, Germany), and mouse monoclonal anti-α-tubulin (clone 6A204, Santa Cruz Biotechnology).

RT-PCR. Total RNA was prepared from HoMel-L1 and HoMel-A1 cells using the RNeasy mini kit (Qiagen, Valencia, CA) according to manufacturer's recommendations, including

on-column DNase digestion with RNase free DNase (Qiagen). The RNA was eluted in RNase-free water, quantified using a ND100 spectrophotometer (NanoDrop Technologies, Inc., Wilmington, DE), and stored at −70°C. First-strand complementary DNA (cDNA) synthesis was performed using the Advantage RT-for-PCR kit (BD Biosciences/Clontech, Palo Alto, CA). One microgram total RNA was mixed with oligo$(dT)_{18}$ primers and random hexamers, and reverse transcription was performed according to manufacturer's recommendations. For both cell lines, a control reaction without reverse transcriptase was run in order to detect possible DNA contamination later in the PCR step. The cDNA was diluted in 30 µl DEPEC-treated H_2O, purified with a Chroma Spin TE-10 column (Clontech), aliquoted, and stored at −70°C. The following primers were used to obtain the corresponding equine full length (FL) or partial (P) transcripts: *ASIP* FL forward 5′-GGATGTCATTCACCTGTTCCTGG-3′ and reverse 5′-CACACGAGTGAGCGTGGACGA-3′, *MC1R* FL forward 5′-GCAGGGGCCCCAGAGGAG-3′ and reverse 5′-CTCCACGACGACACGAGGAC-3′, *POMC* FL forward 5′-CTGCTGCTTCAGGCTTCTGT-3′ and reverse 5′-ACCACCACCTCCTCCTCCT-3′, and *c-KIT* P forward 5′-CTCGGCTTTGCCGCGCTCG-3′ and reverse 5′-GTCTAGTTCCGTGGACTCAATGTGG-3′. PCR was performed using a touchdown PCR program (annealing at 63 to 53°C for 7 cycles followed by annealing at 56 or 59°C for 37 cycles) in 25 µl reactions using 200 ng cDNA, 1 M betaine (Sigma-Aldrich), and 0.6U AmpliTaq Gold (Applied Biosystems, Foster City, CA). Products were purified and sequenced with the corresponding PCR primers.

Analysis of p53 mutations. DNA was prepared from HoMel-A1 and HoMel-L1 cells using the DNeasy Blood & Tissue kit (Qiagen). Exons 2–10 of *p53* were PCR-amplified with the following primers: exons 2–3 forward 5′-CTGTGGGAAGCAAAACCAGT-3′ and reverse 5′-GTACCAACTGGAAGCCATGC-3′, exons 4–6 forward 5′-ACGGTCTCCTGACCTTCCA-3′ and reverse 5′-GAGCATGGGAGAAAGTGCTG-3′, exons 7–8 forward 5′-CCCTTCTTACCTGGGTAGTGGT-3′ and reverse 5′-CTGAGCCTAACCTGGCATTT-3′, and exons 9–10 forward 5′-ACTTCTCTGTCCCCCTCCTC-3′ and reverse 5′-CCTGTAGCAAGCAGAGGTTCA-5′.

Statistical analysis. Data were analyzed by Student's *t* test. Statistically significant differences were determined at $P < 0.05$ level.

Results

Establishment of cell lines. The most critical part of the initial optimization of the culturing conditions was the reduction of the melanin content, by extensive washing of the cells in PBS, due to the toxicity of melanin and its byproducts to cells in vitro. In HoMel-A1 cultures, regularly proliferating cells were observed after 3 wk of incubation, whereas in HoMel-L1 cultures, deeply pigmented slowly growing cells appeared at the periphery of tumor fragments after 12 wk. The resulting melanoma cell cultures were subcultured by limited dilution. Permanently growing cells of both established cell lines were routinely subcultured by 1:5 dilution once a wk when plated at a density of 6×10^4 cells/cm^2. The cells frozen in liquid nitrogen at various passages upon recovery maintained their initial morphology and behavior in culture for more than 100 passages.

Morphological and in vitro growth characteristics. Light microscopy showed that the cells of both cell lines ranged in shape from triangular and stellar to spindle-like with dendritic extensions Fig. 1*A*. The cells had a single nucleus with prominent nucleoli. The main difference between the cell lines was the size of the cells, with the HoMel-A1 cells being about 30% smaller than the HoMel-L1 cells. Furthermore, the HoMel-A1 cells had a higher degree of anisokaryosis and anisocytosis Fig 1*B*. Transmission electron microscopy revealed the presence of melanosomes at various developmental stages in both cell lines Fig. 1*C*. Pigmentation decreased in both cell lines during long-term growth in RPMI-1640 medium. However, the melanin synthesis could be restimulated upon addition of tyrosine or phenylalanine, or by reducing the glucose supply.

The calculated population doubling time in the log growth phase was 90 h for HoMel-L1 and 42 h for HoMel-A1, clearly indicating a growth advantage of the latter Fig. 1*D*. Neither of the cell lines required exogenous growth factors for permanent growth. Furthermore, no detrimental effect on cell proliferation was observed upon FCS deprivation. The cells of both cell lines showed no contact inhibition and grew in a tightly packed monolayer.

Determination of chromosome numbers. The chromosome numbers remained constant in both of the cell lines throughout the culturing period as was determined by chromosome counting at different passages. Of 100 metaphases of HoMel-A1 cells, 78% showed near-haploid number of 32 to 38 chromosomes. The remaining metaphases had either 46 (8%), 59(6%), 62 (2%), 64 (7%), or 128 (2%) chromosomes (Fig. 2). Of 100 metaphases of the HoMel-L1 cells, 75% showed near-diploid number of 64 chromosomes. The remaining metaphases ranged from 60 to 72 chromosomes (Fig. 2).

Evaluation of the tumorigenic potential. Both of the cell lines formed colonies in the soft agar assay, showing the anchorage-independent growth ability (Fig. 3*A*). The number of the colonies was roughly equal between the lines; however, HoMel-A1 formed colonies with higher cell counts (although

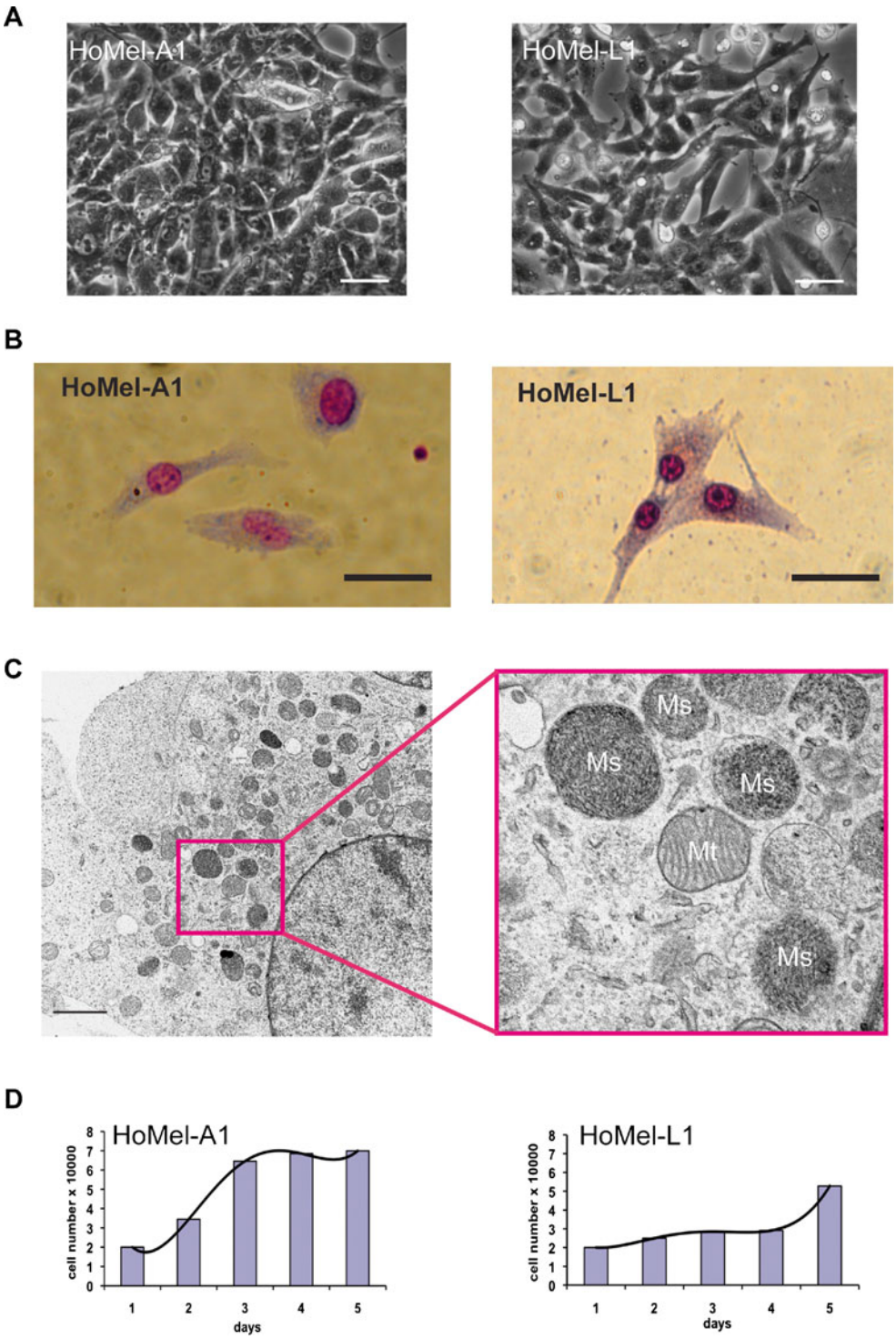

Figure 1. (*A*) Phase contrast microscopy of HoMel-A1 and HoMel-L1 cell cultures. ×40 magnification. *Scale bar*, 18 µm. (*B*) Giemsa–Wright staining of HoMel-A1 and HoMel-L1 cells. ×60 magnification. *Scale bar*, 18 µm. (*C*) Electron microscopy of HoMel-L1 (similar to HoMel-A1). *Mt* mitochondrion, *Ms* melanosome. *Scale bar*, 2 µm. (*D*) Growth curves of the cell cultures. Note a considerably longer lag-phase in HoMel-L1 in comparison to HoMel-A1. Cells were counted at passage 10 as described in Material and Methods.

the difference did not reach statistical significance), suggesting a more aggressive transformation activity (Fig. 3*B*). The in vitro transformed status of the cell lines was strongly matched by their in vivo ability of tumor formation in SCID mice upon subcutaneous injection. Tumors of both cell lines developed at the site of injection in all the injected mice within 8 to 11 d. In consecutive daily observation, the HoMel-A1 cells clearly showed a stronger tumorigenic potential, characterized by faster tumor growth (Fig. 3*C*). After 9 weeks, the maximal HoMel-A1 tumor diameter was 24.5 mm, whereas that of the HoMel-L1 tumor was 19.7 mm ($P < 0.05$). From this stage, the HoMel-A1 tumors stopped gaining in volume in comparison to the HoMel-L1 tumors. None of the tumors progressed to metastasis. In line with a higher tumorigenicity, HoMel-A1 cells also showed a higher invasion capacity in Matrigel invasion assay. The invasiveness of the cells of both

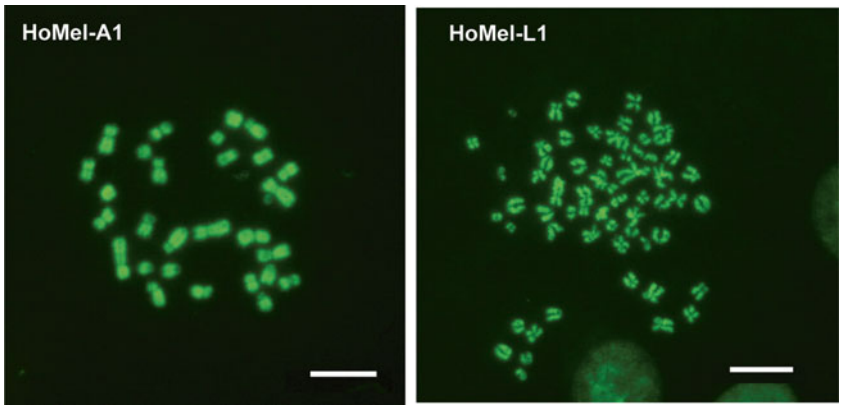

Figure 2. Metaphase chromosome spreads from HoMel-L1 and HoMel-A1 were stained with quinacrine-HCl and chromosome numbers were counted. A representative metaphase spread of HoMel-A1 with haplod set of chromosomes (*left*) and HoMel-L1 with diploid set of chromosomes (*right*). *Scale bar*, 10 μm.

lines was determined as the percentage of cells that can penetrate the control insert relative to the Matrigel insert. About 10 to 28% of HoMel-L1 cells penetrated the Matrigel compared to the control insert. In contrast, about 55 to 88% cells of HoMel-A1 could migrate through the Matrigel insert compared to the control insert (Fig. 3*D*).

Expression of melanocyte- and melanoma-associated antigens. To ascertain that the established cell lines are of melanocytic origin and to test for potential differences between the lines, we examined expression of melanocyte- and melanoma-associated antigens using indirect immunofluorescence (IF). As shown in Fig. 4, both cell lines expressed MITF, TYR, TRP1, PMEL, and AP-2α. The protein expression patterns were similar between lines, except for the apparent reduction in the expression of the melanoma marker AP-2α in HoMel-A1 (Fig. 4*A*). The IF results were confirmed by RT-PCR (data not shown). In addition, we analyzed the mRNA expression of other melanocyte/melanoma-related antigens for which functional antibodies were not available. RT-PCR products of the expected sizes were generated for *ASIP*, *MC1R*, *POMC*, and *KIT* transcripts in both cell lines

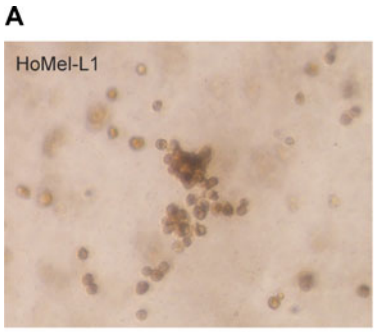

B

Colony forming efficiency

	number of colonies[a]	cells/colony[b]
HoMel-L1	13 ± 1	45.8 ± 5.2
HoMel-A1	14 ± 1	59.6 ± 11.9

[a,b] mean ± SD of 3 experiments

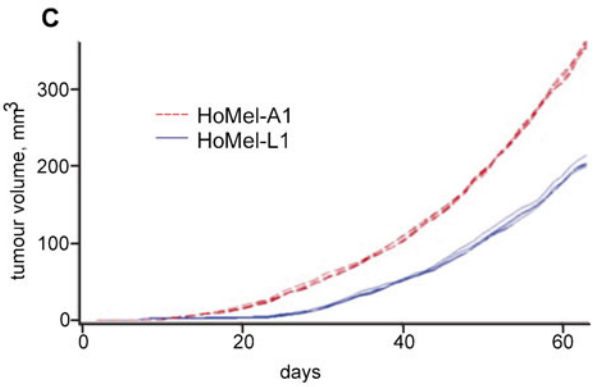

D

Matrigel invasion assay

	number of cells/insert[a]		
	control	matrigel	invasion (%)
HoMel-A1	22.3 ± 14.1	16.5 ± 13.7	74.2
HoMel-L1	8.2 ± 2.0	1.5 ± 0.2	18.1

[a] mean ± SD of 2 experiments in sextuplicates

Figure 3. In vitro and in vivo tumorigenic potential of HoMel-A1 and HoMel-L1 cells. (*A*, *B*) Colony formation assay in soft agar. Representative images of colonies for HoMel-A1 and HoMel-L1 cell lines (A) and quantification of colony-formation efficiency (B). ×40 magnification. (*C*) Tumor in vivo growth in SCID mice. Shown are tumor volumes for tumors formed by subcutaneous inoculations of 1.5×10^6 cells. Each line represents an individual animal. The data shown is representative of one of three independent experiments. (*D*) Quantification of invasiveness of HoMel-A1 and HoMel-L1 cells measured by Matrigel invasion assay.

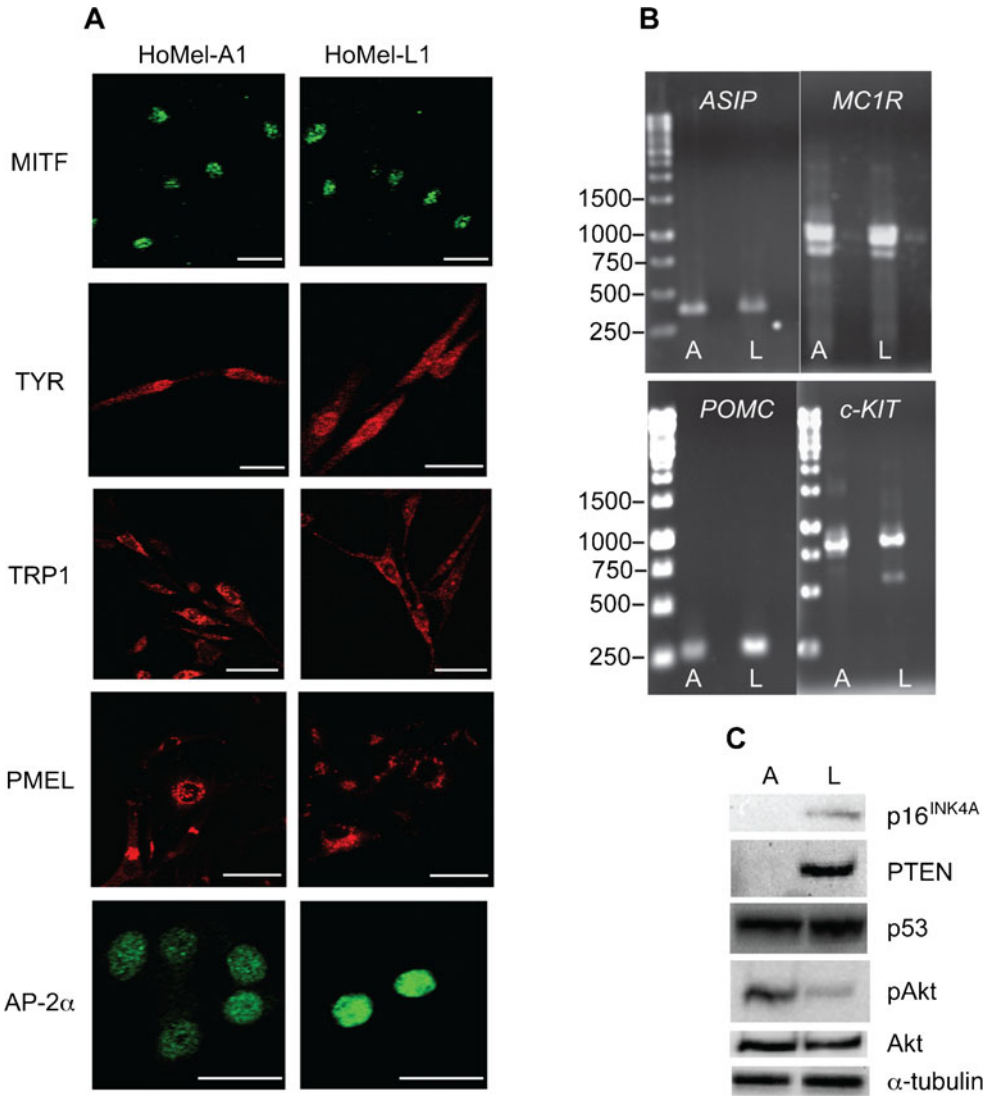

Figure 4. Expression of melanocyte and melanoma antigens in HoMel-A1 and HoMel-L1 cells. (*A*) Immunofluorescence with antibodies against MITF, TYR, TRP1, PMEL, and AP-2α in HoMel-A1 (*left panel*) and HoMel-L1 (*right panel*). *Scale bar*, 20 μm. (*B*) RT-PCR analysis of the expression of *ASIP*, *MC1R*, *POMC*, and *KIT* transcripts in HoMel-A1 (*A*) and HoMel-L1 (*L*). The RT-PCR products were run on 1% agarose gel stained with ethidium bromide. *C* Expression of tumor suppressors $p16^{INK4A}$, PTEN, and p53 and activation of the Akt pathway analyzed by Western blotting in HoMel-A1 (*A*) and HoMel-L1 (*L*).

(Fig. 4*B*). The identity of the PCR products was confirmed by sequencing.

Tumor suppressor profiling. Expression of tumor suppressors $p16^{INK4A}$, p53, and PTEN is often lost or altered in metastatic melanomas (Hearing and Leong 2006). To test for potential alterations in the expression of these proteins in our cell lines, we used Western blot analysis. We found that both $p16^{INK4A}$ and PTEN were lost in HoMel-A1, while these proteins were present in HoMel-L1 (Fig. 4*C*). Loss of PTEN has been linked to the activation of PI3K/Akt signaling in human melanomas (Hearing and Leong 2006), and, in line with this, we detected a higher level of the activated Akt (pAkt) in HoMel-A1 in comparison to HoMel-L1 (Fig. 4*C*). Strong p53 protein expression was detected in both HoMel-L1 and HoMel-A1 cells (Fig. 4*C*). Since the antibody we used here (Pab240) detects both the wild type and mutant forms of the p53 protein, it was not clear which form is expressed in our cell lines. We therefore screened for mutations in exons 2–10 of *p53* by direct sequencing of the corresponding PCR products amplified from genomic DNA. No p53 mutation was detected in either of the cell lines.

Discussion

We report here the establishment and comparative characterization of two novel cell lines, designated HoMel-L1 and HoMel-A1, derived from a primary and a metastatic melanoma tumor of a Grey Lipizzaner and an Arabian horse, respectively. Given that the primary cause for the development of the Grey phenotypes including melanoma is the *Grey* mutation (Rosengren Pielberg et al. 2008; Sundström et al. 2012), a direct comparison of different tumors should be possible. In addition, the fact that both of the cell lines are heterozygous

for the *Grey* mutation (Rosengren Pielberg et al. 2008; Sundström et al. 2012), combined with the close genetic relationship between the Lipizzaner and Arabian breeds (Dovc et al. 2004; Luis et al. 2007), should further minimize background genetic differences to enable comparative studies. Establishment of cell cultures from primary GHMs has been previously described (Chapman et al. 2009). To the best of our knowledge, this study describes the first cell line from a metastatic GHM tumor. Cell lines may change during extended culture periods and not always possess the characteristics of the parental tumor. It is therefore important that both of our GHM cell lines stably maintained their initial characteristics throughout the culturing period as confirmed by various analyses at early and later passages.

In efforts to define changes occurring during progression of GHM, we examined the established cell lines for their growth and morphological characteristics, oncogenic potential, karyotypes, and expression of melanocytic antigens and tumor suppressors. Both of the cell lines displayed characteristics of malignancy, confirming the pathology diagnosis of the parental tumors. The population doubling time for the metastatic HoMel-A1 was less than half of that for the primary HoMel-L1, in line with the higher proliferation indexes observed in human metastatic melanomas in relation to their primary counterparts (i.e., Guerriere-Kovach et al. 2004). The cells of both cell lines had similar morphologies, although the HoMel-A1 cells were smaller and had a higher degree of anisokaryosis and anisocytosis. The degree of pigmentation in both cell lines was considerably lower than that in the parental tumors, and depended on media conditions, as previously described for other GHM as well as canine melanoma cell cultures (Koenig et al. 2001; Chapman et al. 2009).

Both of the cell lines were clearly tumorigenic as demonstrated by their abilities to grow under anchorage-independent conditions by forming colonies in soft agar and induce tumor formation in SCID mice. In line with a more malignant character of the HoMel-A1 cells, these tumors had a stronger oncogenic potential characterized by a faster growth and larger tumor size as compared to the tumors formed by the HoMel-L1 cells. The fact that none of the HoMel-A1 tumors developed metastasis may potentially be attributable to the method of delivery, as it has been previously established that subcutaneously injected melanoma cell lines only very rarely give rise to metastasis. A further testing with intravenous inoculations may help to elucidate whether the blood-borne GHM cells are able to metastasize in SCID/nude mice. In line with the metastatic characteristics of the HoMel-A1 parental tumor, the cells of this line demonstrated a high invasive potential compared to HoMel-L1, as assessed by Matrigel invasion assay. Our in vitro data, therefore, showed a close match to the in vivo characteristics of the parental tumors.

Chromosome counting revealed a striking difference in ploidy between the cell lines, with a near-diploid and a near-haploid modal chromosome number in HoMel-L1 and HoMel-A1, respectively. Previous cytogenetic studies have indicated that genetic abnormalities increase in severity with clinical progression of melanoma (Herlyn et al. 1990; Tlsty et al. 1995). These abnormalities often manifested as progressive aneuploidy as observed in the HoMel-A1 cell line. There are, however, very few reports about a stable haploid cell line developed from a solid tumor, although a hypodiploid DNA pattern in a variety of human tumors (including melanoma) has been found to correlate with a worse prognosis (Atkin and Baker 1981; Toti et al. 1998). Interestingly, previous studies have revealed that both copies of the *STX17* locus on chromosome 25 are maintained in both cell lines as they are heterozygous at this locus (Rosengren Pielberg et al. 2008; Sundström et al. 2012).

The detection of melanocytic markers such as TYR, TRP1, MITF, and PMEL confirmed the melanocytic origin of the lines and showed no discernible difference in the expression pattern between the lines. However, the expression of a melanoma antigen AP-2α, a transcription factor with an established role in the progression of human melanoma (Bar-Eli 1999), was reduced in HoMel-A1, suggesting its potential link to GHM progression. We used RT-PCR to analyze the expression of other melanocyte- and melanoma-associated antigens such as *MC1R*, *ASIP*, *POMC*, and *KIT*, for which no antibodies were available. The mRNA transcripts of these genes were readily detectable in both cell lines.

In humans and mice models, melanoma progression is often associated with reduction or loss of expression of the tumor suppressor $p16^{INK4A}$ (Bennett 2003; Kannan et al. 2003; Monahan et al. 2010). Here, $p16^{INK4A}$ was detected by immunoblotting in HoMel-L1 but absent in HoMel-A1, in line with its loss in the later stages of human melanomagenesis. Expression of another important tumor suppressor, p53, whose functional inactivation with the consequent accumulation of the protein has been associated with progression of human, mouse, and zebrafish melanoma (Sharpless et al. 2003; Patton et al. 2005; Goel et al. 2009; Yu et al. 2009), was strong in both lines. Since the antibody we used can recognize both the wild-type and mutant forms of the p53 protein, it is possible that the observed accumulation of p53 is due to the presence of mutated protein forms as found in some melanomas (Castresana et al. 1993; Ragnarsson-Olding et al. 2002). However, sequencing of the *p53* gene revealed no mutations in either of the cell lines, indicating that other mechanisms are responsible for the observed accumulation of the protein.

In human melanoma, the PI3K/Akt pathway activation via loss of a tumor suppressor PTEN is linked to acquisition of insensitivity to apoptosis and progression to metastases (reviewed in Yajima et al. 2012). Consistently, we found PTEN loss and concurrent activation of the Akt pathway in HoMel-A1 but not in HoMel-L1, thus suggesting that the

pathways similar to those found in human melanoma operate also in GHM.

Previously, we found that a higher copy number of the *STX17* duplication is associated with more malignant GHM tumors, and HoMel-A1 was found to have 5–8 copies of the duplicated sequence in contrast to HoMel-L1 with three copies (Sundström et al. 2012). These cell lines, therefore, are useful to study the link between the presence of the *STX17* duplication and GHM development.

It should be noted that, although the established cell lines stably maintained their initial characteristics, there still might be a possibility that some of the cytogenetic and/or expressional changes we observed were the consequences of an in vitro selection and progression, instead of a true representation of the situation in vivo. Complementary analysis on the in vivo tumors at the appropriate stages will, therefore, be needed.

In conclusion, our in vitro model system will be an important tool for further dissection of the molecular mechanisms behind GHM development and progression as well as an appropriate model for testing new therapeutical strategies for the melanoma treatment.

Acknowledgment The anti-PMEL antibodies were kindly provided by Dr. Michael S. Marks (University of Pennsylvania, Philadelphia, PA). The study was supported by the Swedish Cancer Society (project number CAN 2011/703) and Swedish-Norwegian Foundation for Equine Research (project number H1047299).

References

Atkin N. B.; Baker M. C. A metastatic malignant melanoma with 24 chromosomes. *Hum Genet* 58: 217–219; 1981.

Bar-Eli M. Role of AP-2 in tumor growth and metastasis of human melanoma. *Cancer Metastasis Rev* 18: 377–385; 1999.

Bennett D. C. Human melanocyte senescence and melanoma susceptibility genes. *Oncogene* 22: 3063–3069; 2003.

Castresana J. S.; Rubio M. P.; Vazquez J. J.; Idoate M.; Sober A. J.; Seizinger B. R.; Barnhill R. L. Lack of allelic deletion and point mutation as mechanisms of p53 activation in human malignant melanoma. *Int J Cancer* 55: 562–565; 1993.

Cengelli F.; Grzyb J. A.; Montoro A.; Hofmann H.; Hanessian S.; Juillerat-Jeanneret L. Surface-functionalized ultrasmall superparamagnetic nanoparticles as magnetic delivery vectors for camptothecin. *ChemMedChem* 4: 988–997; 2009.

Chapman S. W. K.; Metzger N.; Grest P.; Feige K.; von Rechenberg B.; Auer J. A.; Hottiger M. O. Isolation, establishment, and characterization of ex vivo equine melanoma cell cultures. *In Vitro Cell Dev Biol Anim* 45: 152–162; 2009.

Dovc P.; Susnik S.; Snoj A. Experience from Lipizzan horse and salmonid species endemic to the Adriatic river system. Examples for the application of molecular markers for preservation of biodiversity and management of animal genetic resources. *J Biotechnol* 113: 43–53; 2004.

Fleury C.; Berard F.; Balme B.; Thomas L. The study of cutaneous melanomas in Camargue-type gray-skinned horses (1): clinical-pathological characterization. *Pigment Cell Res* 13: 39–46; 2000.

Goel V. K.; Ibrahim N.; Jiang G.; Singhal M.; Fee S.; Flotte T.; Westmoreland S.; Haluska F. S.; Hinds P. W.; Haluska F. G. Melanocytic nevus-like hyperplasia and melanoma in transgenic BRAFV600E mice. *Oncogene* 28: 2289–2298; 2009.

Gorham S, Robl M (1986) Melanoma in the Gray Horse - the Darker Side of Equine Aging. Veterinary Medicine 81: 446-&.

Guerriere-Kovach P. M.; Hunt E. L.; Patterson J. W.; Glembocki D. J.; English 3rd J. C.; Wick M. R. Primary melanoma of the skin and cutaneous melanomatous metastases: comparative histologic features and immunophenotypes. *Am J Clin Pathol* 122: 70–77; 2004.

Hearing JV, Leong SPL (2006) From Melanocytes to Melanoma: The Progression to Malignancy Humana Press Totowa, New Jersey.

Herlyn D.; Iliopoulos D.; Jensen P. J.; Parmiter A.; Baird J.; Hotta H.; Adachi K.; Ross A. H.; Jambrosic J.; Koprowski H.; Herlyn M. In vitro properties of human melanoma cells metastatic in nude mice. *Cancer Res* 50: 2296–2302; 1990.

Kannan K.; Sharpless N. E.; Xu J.; O'Hagan R. C.; Bosenberg M.; Chin L. Components of the Rb pathway are critical targets of UV mutagenesis in a murine melanoma model. *Proc Natl Acad Sci USA* 100: 1221–1225; 2003.

Koenig A.; Wojcieszyn J.; Weeks B. R.; Modiano J. F. Expression of S100a, vimentin, NSE, and melan A/MART-1 in seven canine melanoma cells lines and twenty-nine retrospective cases of canine melanoma. *Vet Pathol* 38: 427–435; 2001.

Luis C.; Juras R.; Oom M. M.; Cothran E. G. Genetic diversity and relationships of Portuguese and other horse breeds based on protein and microsatellite loci variation. *Anim Genet* 38: 20–27; 2007.

MacGillivray K. C.; Sweeney R. W.; Del Piero F. Metastatic melanoma in horses. *J Vet Intern Med* 16: 452–456; 2002.

Monahan K. B.; Rozenberg G. I.; Krishnamurthy J.; Johnson S. M.; Liu W.; Bradford M. K.; Horner J.; Depinho R. A.; Sharpless N. E. Somatic p16(INK4a) loss accelerates melanomagenesis. *Oncogene* 29: 5809–5817; 2010.

Patton E. E.; Widlund H. R.; Kutok J. L.; Kopani K. R.; Amatruda J. F.; Murphey R. D.; Berghmans S.; Mayhall E. A.; Traver D.; Fletcher C. D.; Aster J. C.; Granter S. R.; Look A. T.; Lee C.; Fisher D. E.; Zon L. I. BRAF mutations are sufficient to promote nevi formation and cooperate with p53 in the genesis of melanoma. *Curr Biol* 15: 249–254; 2005.

Ragnarsson-Olding B. K.; Karsberg S.; Platz A.; Ringborg U. K. Mutations in the TP53 gene in human malignant melanomas derived from sun-exposed skin and unexposed mucosal membranes. *Melanoma Res* 12: 453–463; 2002.

Raposo G.; Tenza D.; Murphy D. M.; Berson J. F.; Marks M. S. Distinct protein sorting and localization to premelanosomes, melanosomes, and lysosomes in pigmented melanocytic cells. *J Cell Biol* 152: 809–824; 2001.

Rosengren Pielberg G.; Golovko A.; Sundström E.; Curik I.; Lennartsson J.; Seltenhammer M. H.; Druml T.; Binns M.; Fitzsimmons C.; Lindgren G.; Sandberg K.; Baumung R.; Vetterlein M.; Stromberg S.; Grabherr M.; Wade C.; Lindblad-Toh K.; Ponten F.; Heldin C. H.; Solkner J.; Andersson L. A cis-acting regulatory mutation causes premature hair graying and susceptibility to melanoma in the horse. *Nat Genet* 40: 1004–1009; 2008.

Seltenhammer M. H.; Heere-Ress E.; Brandt S.; Druml T.; Jansen B.; Pehamberger H.; Niebauer G. W. Comparative histopathology of Grey horse melanoma and human malignant melanoma. *Pigment Cell Res* 17: 674–681; 2004.

SAS Institute Inc. Base SAS(R)9.2 Procedures Guide. Cary, NC: SAS Institute Inc. 2011.

Sharpless N. E.; Kannan K.; Xu J.; Bosenberg M. W.; Chin L. Both products of the mouse Ink4a/Arf locus suppress melanoma formation in vivo. *Oncogene* 22: 5055–5059; 2003.

Sundström E.; Imsland F.; Mikko S.; Wade C.; Sigurdsson S.; Pielberg G. R.; Golovko A.; Curik I.; Seltenhammer M. H.; Solkner J.; Lindblad-Toh K.; Andersson L. Copy number expansion of the

STX17 duplication in melanoma tissue from Grey horses. *BMC Genomics* 13: 365; 2012.

Sundström E.; Komisarczuk A. Z.; Jiang L.; Golovko A.; Navratilova P.; Rinkwitz S.; Becker T. S.; Andersson L. Identification of a melanocyte-specific, microphthalmia-associated transcription factor-dependent regulatory element in the intronic duplication causing hair graying and melanoma in horses. *Pigment Cell Melanoma Res* 25: 28–36; 2011.

Sutton R. H.; Coleman G. T. Melanoma and the Graying horse. RIRDC Research, Paper Series Barton, Australia; 1997.

Tlsty T. D.; Briot A.; Gualberto A.; Hall I.; Hess S.; Hixon M.; Kuppuswamy D.; Romanov S.; Sage M.; White A. Genomic instability and cancer. *Mutat Res* 337: 1–7; 1995.

Toti P.; Greco G.; Mangiavacchi P.; Bruni A.; Palmeri M. L.; Luzi P. DNA ploidy pattern in choroidal melanoma: correlation with survival. A flow cytometry study on archival material. *Br J Ophthalmol* 82: 1433–1437; 1998.

Valentine B. A. Equine melanocytic tumors: a retrospective study of 53 horses (1988 to 1991). *J Vet Intern Med* 9: 291–297; 1995.

Yajima I.; Kumasaka M. Y.; Thang N. D.; Goto Y.; Takeda K.; Yamanoshita O.; Iida M.; Ohgami N.; Tamura H.; Kawamoto Y.; Kato M. RAS/RAF/MEK/ERK and PI3K/PTEN/AKT signaling in malignant melanoma progression and therapy. *Dermatol Res Pract* 2012: 354191; 2012.

Yu H.; McDaid R.; Lee J.; Possik P.; Li L.; Kumar S. M.; Elder D. E.; Van Belle P.; Gimotty P.; Guerra M.; Hammond R.; Nathanson K. L.; Dalla Palma M.; Herlyn M.; Xu X. The role of BRAF mutation and p53 inactivation during transformation of a subpopulation of primary human melanocytes. *Am J Pathol* 174: 2367–2377; 2009.